



# Optimal Design of Body Profile for Stable Stair Climbing Via Tri-wheels

Younghwan Kim<sup>1</sup> · Donghan Son<sup>1</sup> · Jeongpil Shin<sup>1</sup> · Taewon Seo<sup>1</sup>

Received: 1 January 2023 / Revised: 16 August 2023 / Accepted: 17 August 2023 / Published online: 13 September 2023  
© The Author(s), under exclusive licence to Korean Society for Precision Engineering 2023

## Abstract

In this paper, we propose a mobile robot platform that is an improved form of LEVO. The LEVO uses a regular wheel and curved spoke triwheel(CSTW) system to drive flat terrain and stair climbs. However, this robot has problems when climbing stairs: it's bottom profile collides with the stairs, resulting in huge jerk. To solve this problem, in this study, attempts to reduce the jerk value by applying a blade using a B-spline to the bottom profiles where the robot collides with the stairs. At this time, by reducing jerk, it can contribute to extending the life of the robot and improving driving stability. This study involved two steps. First, simulation was performed by adjusting the number and position of control points of the curve (B-spline). In this process, the orthogonal arrangement was applied among the optimal design techniques to finally reduce the jerk value by 92% and the driving torque needed to climb the stairs by 9.5%. At this time B-spline has one control point and the position is (300, 15). This simulation result was verified experimentally using a test bench and a prototype robot. As a result, it was confirmed that the jerk was reduced by 66.7%. Simulations and experimental verification based on them have shown that the proposed method is sufficiently effective in real environment.

**Keywords** Stair-climbing · Last mile-delivery robot · Jerk reduction · Optimal design

## 1 Introduction

Owing to the COVID-19 pandemic, the popularity of online markets has increased significantly, which, in turn, has led to the growth of the last-mile delivery market. According to a survey by global research “GlobalData” [1], the proportion of e-commerce in Korea is continuously increasing. With regard to global trends, online markets constitute 40% of all markets in countries such as the United States, China, and Germany [2]. Moreover, global market research “Maximize” predicts that the last-mile delivery market will continue to grow [3]. However, such a rapid growth of the market may

result in excessive workloads for delivery services, resulting in additional accidents among courier workers and an increase in traffic volumes for the general public.

In this regard, last-mile delivery robots have emerged as a solution to the aforementioned problems [4]. Like pioneer 3-DX [5], these robots perform their own tasks based on path-planning. Among these, the most popular robot is the wheeled-robot; representative examples, include Scout-Amazon [6] and Delidrive-Hyundai [7], developed by Bae-dal Minjok and Hyundai Robotics in-line with the rapidly growing Korean delivery market.

These robots are navigated using wheels and offer the advantages of high speeds and stability when driving on the ground; however, they also face difficulties in overcoming obstacles such as stairs. In this regard, in countries where single-family houses constitute the social housing environment, there are few obstacles along the paths to the houses. Hence, the existing wheeled-robots can be easily employed. By contrast, in certain areas of Korea, where obstacles such as stairs are relatively common because the residential environment is primarily composed of apartments, this type of robot is difficult to commercialize. Considering this situation in Korea, in this work, a mobile robot capable of overcoming

---

✉ Taewon Seo  
taewonseo@hanyang.ac.kr

Younghwan Kim  
guma97@hanyang.ac.kr

Donghan Son  
ddh1597@gmail.com

Jeongpil Shin  
jpshin9743@gmail.com

<sup>1</sup> Department of Mechanical Convergence Engineering,  
Hanyang University, 222, Wangsimni-ro, Seongdong-gu,  
Seoul 04763, Republic of Korea

stairs was studied, and a last-mile delivery robot platform was accordingly developed.




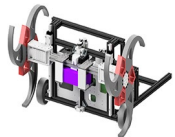
Prior to explaining the reference model employed to realize the aforementioned prototype robot, we first examine the mechanism of a typical stair-overcoming robot. In this work, four major types of robots were compared. As presented in Table 1, the first robot considered was sTero [8], which features a detachable body platform [9]. Although this robot exhibits stable running and stair-overcoming performances, it also shows significant differences in the overcoming speed, as compared to other robots, owing to the complexity of its stair-overcoming mechanism. The second robot considered was Spot-mini [10], which is regarded as a representative legged-robot [11]. A legged-robot overcomes stairs via the mechanism of “walking,” therefore, it overcomes stairs in the form most similar to that of humans. As stairs constitute an environment tailored to humans, this type of robot can be regarded as the most suitable form of overcoming stairs based on human-like “walking.” However, this robot is relatively difficult to control and involves significant research costs. Furthermore, the third robot considered was the tracked-robot [12], which is inspired by caterpillars and capable of overcoming stairs as well as various other types of obstacles. However, compared to wheel-based robots, this type of robot suffers from disadvantages such as slow speeds and instability during ground driving. The last type of robot considered was a tri-wheel-switching robot, i.e., LEVO [13–15]. LEVO features a switching system as a base; it is also equipped with wheels for ground driving and curved-spoke tri-wheels (CSTW) [16] to overcome stairs. Thus, this robot offers the advantage of being capable of both overcoming stairs and driving on the ground. Although it has a

particularly low design complexity, it shows an advantage over other robots in terms of speed to overcome stairs. The abovementioned comparisons are summarized in Table 1. Based on these results, LEVO was selected as the basic model in this study.

LEVO achieved satisfactory results for all the evaluation indices used to compare the stair-overcoming mechanisms. However, LEVO suffers from a disadvantage. Unlike the other robots, when overcoming stairs using the CSTW, its body is dragged. Under these conditions, the bottom surface of the robot and the stairs collide. When such a collision occurs, the acceleration of the robot is altered, which is indicated by a sudden change in the jerk value. In this case, the jerk value is a derivative of the acceleration. A large jerk value may result in a reduction in the life of the internal motor and its various components [17]. This occurrence of jerks as well as the collisions can cause damage to the goods, which, in turn, can be a significant disadvantage when developing mobile robot platforms aimed at last-mile delivery.

To address these limitations, in this study, the floor surface of the robot was redesigned to reduce the impact from the collision with stairs. The cam curve is considered as an example in the process of redesigning the shape. When designing the cam, the designer aims to maintain the continuity of the velocity and acceleration by utilizing a B-spline curve [18]. And, if the floor surface is set to a curved surface, the angle of the force acting between the robot floor surface and the edge of the stairs at the time of a collision approaches 0 degree, so it has the effect of reducing the amount of speed change, that is, the amount of impact applied to the robot [19]. Before applying the above phenomena to the robot, we reviewed and analyzed how to draw

**Table 1** Comparison of stairway overcoming mechanisms

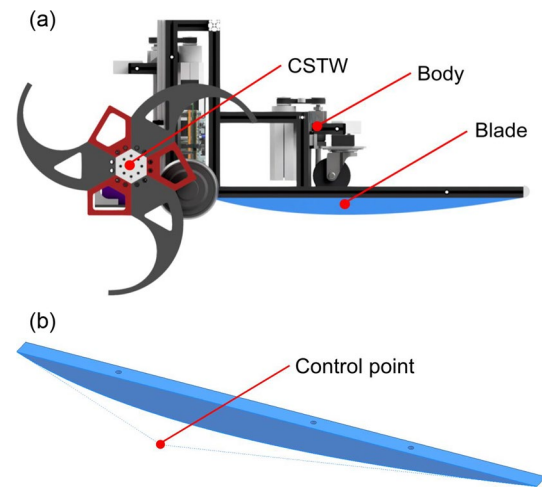
| Mechanism              | Detachable body platform  | Legged-robot  | Tracked-robot   | Tri-wheel switching robot   |
|------------------------|---|---|---|---|
|                        |  |  |  |  |
| Name                   | sTero [8]   | Spot-mini [10]  | Tracked-robot [12]  | LEVO [13]   |
| Operation stability    | +   | +   | –   | +   |
| Field driving          | +   | –   | –   | +   |
| Control                | +   | –   | +   | +   |
| Design complexity [16] | –   | –   | +   | +   |
| Climbing speed         | 0.3 step/s  | 1 step/s  | 1 step/s  | 1.47step/s  |
| Limitation             | slow stair overcoming speed   | Complicated structure   | Edge contact  | –   |

curves to determine the most suitable method. The characteristics of the seven representative curve design methods, which were analyzed in this study, are presented in Table 2. Because the B-spline and higher-order equations are commonly used as a method for designing curves, only these two are representatively compared in detail. First, in the case of higher-order equations, a curve can be simply designed using coefficients alone; however, there exists a disadvantage in that vibrations occur owing to the difference compared to the actual curve. Conversely, the B-spline offers the advantage of being easy to draw in a cad environment [20] and allows for relatively fine adjustments based on regionality; therefore, the B-spline was selected for application. Compared with the other five curves, the B-spline features regionality, making it possible to fine-tune the curve; it was selected because it was the most suitable for this study in terms of all aspects, such as the continuity during differentiating and vibration.

In this work, we aimed to reduce the amount of impact generated between the stairs by changing the floor surface of the robot from a straight structure (as employed in LEVO) to a curved structure by attaching the designed blade. A stair with a width and a height of 300 mm and 160 mm, respectively, was set as the target overcoming environment. To confirm that this change can sufficiently reduce jerk and vibration, which significantly affect the life of the robot, a simulation was conducted. The derived results were then applied to improve LEVO and test it under an actual environment to verify the research performance.

## 2 Configuration of LEVO

Figure 1a shows the hardware configuration of LEVO equipped with the blade, and Fig. 1b shows the 3D-design of the blade and control point, which is a design variable. The robot used in this experiment is mainly composed of



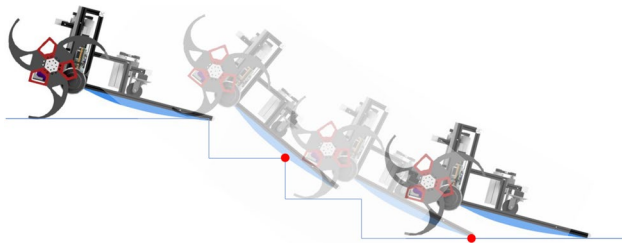
**Fig. 1** a Overall hardware structure of LEVO and b 3D-design of blade and B-spline control point

three parts: the main body, which is the robot’s overall frame; a triangular wheel module to overcome stairs; and a bottom blade, which was optimized in this study. The component that was additionally attached to the floor profile to alter the shape of the contact surface between the stairs and the robot is referred to as the “blade.”

These aspects have been explained in detail. First, the CSTW module consists of a CSTW and a motor to climb stairs. Only the power supplied by this motor is used to overcome stairs; the blade serves solely as a support. A friction pad is attached to the contact surface of the curved spoke to overcome stairs more easily. Acrylic (MA) with a low coefficient of friction was used for the blade, as summarized in Table 3. Figure 2 illustrates the process of the robot overcoming stairs. Additionally, during this process, the contact point between the stairs and floor surface of the robot varies. Lastly, the body includes a robot frame and a switching module with a wheel for ground driving.

**Table 2** Types and characteristics of curves

| Type of curve         | First differential | Second differential | Vibration                                    | Defined variable                      | Regionality |
|-----------------------|--------------------|---------------------|--|---------------------------------------|-------------|
| Straight line         | Discontinuity      | Discontinuity       | –  | Panel point                           | o           |
| High-order polynomial | Continuity         | Continuity          | Heavy  | Panel point                           | x           |
| Cubic spline          | Continuity         | Continuity          | Existing                                     | Panel point                           | x           |
| Hermite curve         | Continuity         | Discontinuity       | It depends on the, differential coefficient. | Panel point, differential coefficient | o           |
| Osculating polynomial | Continuity         | Continuity          | It depends on the, differential coefficient. | Panel point, differential coefficient | o           |
| Bezier curve          | Continuity         | Continuity          | Existing                                     | Control point                         | x           |
| B-Spline curve        | Continuity         | Continuity          | existing                                     | Control point                         | x           |



**Fig. 2** Step-overcoming process of LEVO

**Table 3** Type of flooring and coefficient of friction

| Item              | Specification   | Friction coefficient |
|-------------------|-----------------|----------------------|
| ACRYLIC           | MA              | 0.38                 |
| Anti-friction pad | STHVSA4-300-300 | 0.97                 |

## 3 Blade Design and Optimization

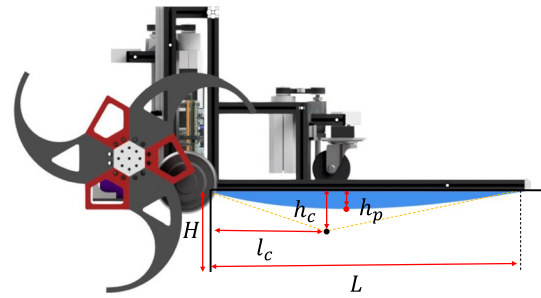
### 3.1 Blade Design

The blade was designed using a B-spline. The B-spline does not require interpolation to adjust the curve, because the control point is not located at the top of the curve. Additionally, when moving one control point, only the section around the control point is moved, owing to regionality; thus, it is advantageous for fine curve adjustments. The formula [21] for the B-spline is expressed as follows:

$$S(u) = \sum_{i=0}^n N_{i,p}(u)P_i \quad (0 \leq u \leq 1) \quad (1)$$

$$N_{i,0}(u) = \begin{cases} 1 & \text{if } u_i \leq u \leq u_{i+1} \\ 0 & \text{otherwise} \end{cases} \quad (2)$$

The design parameters considered for the design of the curve of the blade in this study are presented in Fig. 3. These variables can be broadly divided under the following three categories. First,  $H$  and  $L$  indicate that the maximum distance of the control point can move along the vertical and horizontal directions. Second,  $h_c$  and  $l_c$  indicate the location of the control point of the B-spline curve applied to the blade. Here,  $h_c$  is the height between the control point and the lower profile, and  $l_c$  is the distance from the reference point to the control point. The reference point is the starting point of the lower profile. Finally,  $h_p$  represents the height of the highest point on the blade. The blade is designed by varying the location of the control point of the B-spline curve, that is, variables  $h_c$  and  $l_c$ , using Inventor.



**Fig. 3** Design parameters for the blade of LEVO

**Table 4** Optimization problem formulation

| Design variables   | Number of control points, $h_c, l_c$   |
|--------------------|--|
| Objective function | Minimize the jerk and $T_{RMS}$  |
| Constraint         | Number of control points: 1ea, 2ea<br>$-80 \text{ mm} < h_c < 80 \text{ mm}$<br>$0 \text{ mm} < l_c < 605 \text{ mm}$<br>$h_p < 38.5 \text{ mm}$ |

### 3.2 Optimization Problem Formulation

To design a blade with the most suitable dimensions, the design problem for optimization is formulated before proceeding with the optimization. First, the purpose of the simulation was to minimize the jerk that occurs during a collision with the stairs. A total of three design variables were considered in this process, including two independent variables and one dependent variable. The set variable of the control points,  $h_c, l_c$ , acts as an independent variable, whereas the blade's highest point,  $h_p$ , is a dependent variable determined by the independent variable  $h_c, l_c$ . Among these variables,  $h_c$  should not exceed  $H$ , which is the maximum allowable distance along the y-axis, and  $l_c$  should not exceed  $L$ , which is the length of the lower profile of the robot. Moreover, although not directly used in this experiment,  $h_p$  was set to be smaller than the height at which the caster wheel did not interfere with the flat driving mode. This simulation was conducted based on the conditions summarized in Table 4, and the experiment was conducted using the orthogonal array method [22]. The orthogonal array method refers to a finite set of vectors on a given finite set, in which all possible vectors are evenly distributed when constrained to a subset of coordinates in combinatorics. Based on this, it is not to conduct experiments on the entire range of experimental points, but to create experimental points with a combination of certain standards and conduct experiments. In the case of the OA technique, it is a technique that ensures that the function of the whole can be tested with a limited and proportionate amount of combinations without affecting the quality of the experimental results.

### 3.3 Simulation SET-UP

Experiments must be performed to solve the formalized optimization problems. However, directly manufacturing the blades for all test points and attaching them to the robot can be time- and cost-intensive. Therefore, before experimenting under an actual environment, we designed a simplified model that was implemented under conditions similar to those in the actual environment, using commercial simulation tools(RECURDYN); thereafter, simulations were conducted based on this implementation. And in the course of the simulation, the setting values for the environment are as follows. The stiffness and damping coefficient for the contact conditions between the CSTW and the step surface and between the tail mechanism and the step surface were selected as 100000 N/mm and 10 N/mm.s. The climbing speed was unified to 1 step/s (CSTW wheel speed is 20 rpm), and the friction coefficient of the blade was also unified to 0.2, which is the friction coefficient between acrylic and wood. And the sampling time is 0.001 s. Subsequently, based on the derived simulation results, the optimal alternative was determined. We then intended to verify this optimal result through experiments conducted in the actual environment. Therefore, it is necessary to set the simulation environment as close as possible to the actual environment. To this end, based on the Inventor 3D modeling of LEVO, a simplified simulation model including joints was produced.

Here, the values of  $W_1$ ,  $W_2$ , and  $L$  for the size of the robot, as expressed in Fig. 4, are the same, and the values of  $l_{bf}$  and  $h_b$ , which express the position of the center of mass (COM), are also set to be the same as far as possible. Here,  $W_1$  is the distance from the left CSTW to the right CSTW,  $W_2$  is the width of the body profiles, and  $L$  is the total length of the lower body profile.  $l_{bf}$ ,  $h_b$  indicates the distance from the reference point to the COM; a comparison of the exact dimensions is presented in Table 5.

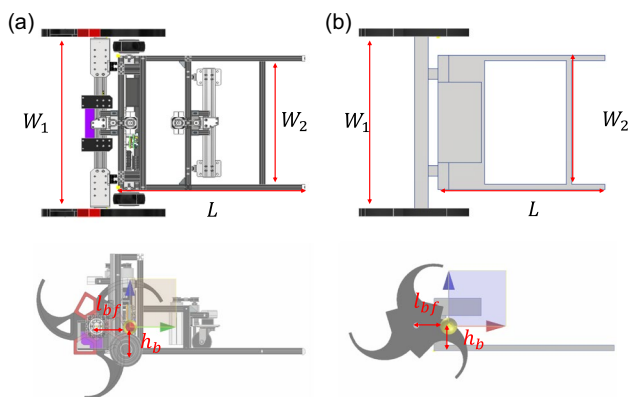


Fig. 4 a Real model and b simplified simulation model

Table 5 Numerical comparison of real model and simplified simulation model

| Variable | Real model (mm) | Simulation model (mm) |
|----------|-----------------|-----------------------|
| $W_1$    | 700             | 700                   |
| $W_2$    | 500             | 500                   |
| $L$      | 605             | 605                   |
| $l_{bf}$ | 108.96          | 108.95                |
| $h_b$    | 83.54           | 83.98                 |

The driving torque,  $T_{RMS}$ , and the average of the change in the amount of jerk are obtained as the output from the simulation. At this time, jerk simply means the amount of change in acceleration with respect to the amount of change in time. Therefore, in order to obtain this, the following equation is generally followed.

$$jerk = \frac{a(t + \Delta t) - a(t)}{\Delta t} = \frac{\Delta a}{\Delta t} \tag{3}$$

In addition, jerk was derived from the simulation as follows. Derive the acceleration change from the obtained acceleration data and calculate it by dividing it by the phase (simulated sampling time) interval of the simulation. In other words, the robot’s acceleration before the stairs and blades collide and the change in acceleration immediately after the collision divided by the change in time.

In this case, the average jerk change,  $J_{avr}$ , indicates the difference between the jerk value at the time of collision with the stairs and the absolute jerk value of the initial model and yields the average of these values. The value of  $J_{avr}$  can be determined as follows:

$$J_{avr} = \sum_{n=2}^5 (|jerk_{initial,n}| - |jerk_{simulation,n}|) / 4 \tag{4}$$

Based on the output  $J_{avr}$ , we can determine the number of control points and the values of  $h_c$  and  $l_c$  that minimize the jerk, which is the objective of this optimization. The range was narrowed, and the simulation was performed. At this time, it was set that the robot moved at a speed of 1 [step/s], and the CSTW wheel driving at a speed of 20 [rpm].

The selected models were inferred to be more effective than the existing models, based on the output  $T_{RMS}$ , average of the generated jerk, and friction coefficient results. To determine whether the final result is sufficiently effective, as compared to the initial values, we compared the average jerk values that occur, instead of  $J_{avr}$ .

The driving torque and friction coefficient were also compared to determine if the robot was operating reliably. The simulation is set up to allow the robot to climb stairs at a constant speed. Therefore, the CSTW wheel must be rotated

at a constant speed of 20 rpm, so the required driving torque and the minimum required friction factor to climb the stairs will vary with time. The drive torque and friction coefficient values are output data derived from a commercial simulation program.

The driving torque comparison to ensure that the robot is climbing the stairs stably is usually determined by the peak value of the driving torque. However, CSTW wheel caused noise in the peak value due to the stopper structure. Therefore, in this study, we wanted to use the RMS value of the driving torque instead of the peak value to determine whether the shape of the blade affects the stable stair driving of the robot. The value of  $T_{RMS}$  can be determined as follows:

$$T_{RMS} = \sqrt{\frac{1}{N} \sum_{i=1}^N (T_i)^2} \quad (5)$$

## 4 Simulation

### 4.1 Simulation with One Control Point

#### 4.1.1 Simulation 1–1

First, simulation 1–1, where a single control point was considered, was performed. Based on the data presented

in Table 4, the orthogonal array optimal design technique was applied.  $l_c$  arranges the range of 0–605 mm into a total of 7 points [0 100 200 300 400 500 600]. And if  $h_c$  has a negative value for the dimensions listed in Table 4, a curve is formed inside the lower profile, such that it does not come into contact with the stairs. In this case, it proceeds by resetting it to 0–80 mm, and five experimental points are designated [0 20 40 60 80]. In this manner, 35 simulated experimental points were generated using the Cartesian coordinate system. In the simulation, jerk data pertaining to the time when the 2nd to 5th stairs collided with the lower part of the robot were extracted. Notably, the data generated when the first column of the stairs collided with the robot were omitted, because, at this instant, the lower body of the robot was still in contact with the floor and not the stairs.

Table 6 lists the jerk values measured as the results of simulation 1–1; based on these values, Fig. 5 is derived. As indicated by the  $l_c, J_{avr}$  graph, there is no evident regularity between the values of  $l_c$  and  $J_{avr}$ . However, as shown in the  $h_c, J_{avr}$  graph, when  $h_c$  is 20 mm, the  $J_{avr}$  value tends to be large. In this case,  $J_{avr}$  is the absolute value difference relative to the initial value; hence, the larger this value, the greater is the jerk. Therefore, it was confirmed that the best result is achieved when  $h_c$  equals 20 mm; this value was considered and further subdivided, and simulation 1–2 was performed.

**Table 6** Result of simulation 1–1 (jerk)

| Position ( $l_c, h_c$ )          | Initial (0, 0) | (0, 20)   | (0, 40)   | (0, 60)   | (0, 80)   | (100, 20) | (100, 40) | (100, 60) | (100, 80) | (200, 20) |
|----------------------------------|----------------|-----------|-----------|-----------|-----------|-----------|-----------|-----------|-----------|-----------|
| 2nd floor ( $\times 10^5$ )      | 7.68           | 0.35      | – 0.49    | –         | –         | – 7.01    | 1.22      | –         | –         | 1.74      |
| 3rd floor ( $\times 10^5$ )      | 5.72           | 0.21      | – 7.14    | –         | –         | – 1.36    | 0.23      | –         | –         | – 13.33   |
| 4th floor ( $\times 10^5$ )      | 6.31           | 5.16      | – 2.41    | –         | –         | 0.30      | – 13.65   | –         | –         | – 12.56   |
| 5th floor ( $\times 10^5$ )      | 7.63           | – 0.78    | – 8.64    | –         | –         | 0.37      | – 1.47    | –         | –         | – 11.43   |
| $J_{avr} (\times 10^5) [mm/s^3]$ | –              | 5.21      | 2.16      | –         | –         | 4.57      | 2.69      | –         | –         | – 2.54    |
| Position ( $l_c, h_c$ )          | (200, 40)      | (200, 60) | (200, 80) | (300, 20) | (300, 40) | (300, 60) | (300, 80) | (400, 20) | (400, 40) | (400, 60) |
| 2nd floor ( $\times 10^5$ )      | 0.25           | –         | –         | – 1.64    | – 0.65    | –         | –         | 0.05      | – 0.88    | – 2.97    |
| 3rd floor ( $\times 10^5$ )      | – 0.21         | –         | –         | – 1.30    | – 5.57    | –         | –         | 0.59      | – 4.92    | – 0.69    |
| 4th floor ( $\times 10^5$ )      | 0.25           | –         | –         | – 1.31    | – 0.78    | –         | –         | – 3.31    | – 3.17    | – 4.90    |
| 5th floor ( $\times 10^5$ )      | – 4.31         | –         | –         | – 1.14    | – 2.68    | –         | –         | 1.13      | – 32.31   | –         |
| $J_{avr} (\times 10^5) [mm/s^3]$ | 5.58           | –         | –         | 5.49      | 4.41      | –         | –         | 5.56      | – 3.49    | –         |
| Position ( $l_c, h_c$ )          | (400, 80)      | (500, 20) | (500, 40) | (500, 60) | (500, 80) | (600, 20) | (600, 40) | (600, 60) | (600, 80) |           |
| 2nd floor ( $\times 10^5$ )      | –              | – 0.99    | 0.30      | – 4.80    | –         | – 0.28    | – 0.98    | – 4.12    | –         |           |
| 3rd floor ( $\times 10^5$ )      | –              | – 4.17    | – 2.30    | – 15.31   | –         | – 1.25    | – 3.25    | – 3.65    | –         |           |
| 4th floor ( $\times 10^5$ )      | –              | 0.29      | – 5.03    | – 2.42    | –         | 0.41      | – 3.45    | – 2.98    | –         |           |
| 5th floor ( $\times 10^5$ )      | –              | – 3.24    | – 4.36    | – 6.42    | –         | 0.26      | – 4.60    | – 4.67    | –         |           |
| $J_{avr} (\times 10^5) [mm/s^3]$ | –              | 4.66      | 3.83      | 1.04      | –         | 6.28      | 3.76      | 2.98      | –         |           |

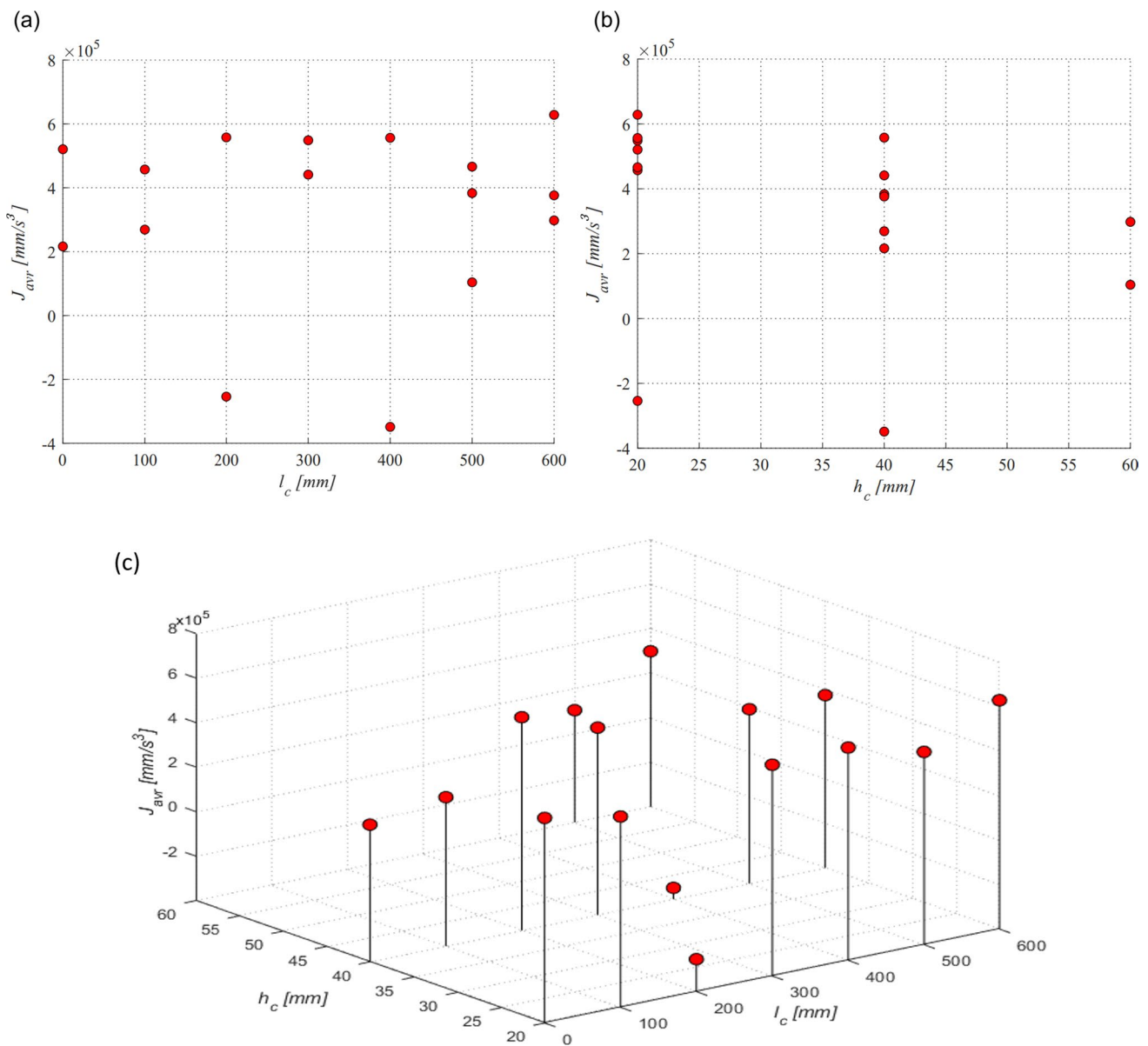


Fig. 5 a  $l_c, J_{avr}$  graph, b  $h_c, J_{avr}$  graph

### 4.1.2 Simulation 1–2

In simulation 1–2, based on the results of simulation 1–1, as discussed above, optimization was repeated considering  $h_c=20$  mm, which afforded the best result in terms of minimizing  $J_{avr}$ . In the case of  $l_c$ , the existing seven points [0 100 200 300 400 500 600] were applied. The range of  $h_c$  was reset as  $15 \text{ mm} < h_c < 25 \text{ mm}$ , by applying three new points [15 20 25]. Accordingly, 21 new orthogonal array test points were created. The subsequent processes proceeded in the same manner as that in simulation 1–1. The results of simulation 1–2 are presented in Table 7.

Based on these results, it was deduced that, in the presence of a single control point, the highest efficiency is achieved at the point where  $(l_c, h_c)$  corresponds to (300, 15). The average of the absolute jerk value,  $T_{RMS}$ , and the friction coefficients at the experimental point were simultaneously compared with those in simulation 2, which included two control points.

### 4.2 Simulation with Two Control Points

Simulations were performed considering the existence of two control points (denoted as Simulation 2). This involved

**Table 7** Result of simulation 1–2 (jerk)

| Position ( $l_c, h_c$ )          | Initial (0, 0) | (0, 15)   | (0, 20)   | (0, 25)   | (100, 15) | (100, 20) | (100, 25) | (200, 15) | (200, 20) | (200, 25) |
|----------------------------------|----------------|-----------|-----------|-----------|-----------|-----------|-----------|-----------|-----------|-----------|
| 2nd floor ( $\times 10^5$ )      | 7.68           | - 8.61    | 0.35      | - 2.90    | - 12.91   | - 7.01    | - 4.47    | - 3.35    | 0.17      | - 17.68   |
| 3rd floor ( $\times 10^5$ )      | 5.72           | - 0.49    | 0.21      | - 1.04    | 0.41      | - 1.36    | - 7.88    | - 0.43    | - 13.33   | 0.38      |
| 4th floor ( $\times 10^5$ )      | 6.31           | - 4.55    | 5.16      | - 8.91    | - 12.22   | 0.30      | - 1.25    | - 0.59    | - 12.56   | - 1.47    |
| 5th floor ( $\times 10^5$ )      | 7.63           | - 0.90    | - 0.78    | - 6.49    | - 14.02   | 0.37      | - 6.26    | - 2.45    | - 11.43   | - 1.40    |
| $J_{avr} (\times 10^5) [mm/s^3]$ | -              | 3.20      | 5.21      | 2.00      | - 3.06    | 4.57      | 1.87      | 5.13      | - 2.54    | 1.60      |
| Position ( $l_c, h_c$ )          | (300, 15)      | (300, 20) | (300, 25) | (400, 15) | (400, 20) | (400, 25) | (500, 15) | (500, 20) | (500, 25) | (600, 15) |
| 2nd floor ( $\times 10^5$ )      | 0.01           | - 1.64    | - 2.62    | - 2.23    | 0.05      | - 2.12    | - 0.31    | - 0.99    | - 5.29    | - 0.65    |
| 3rd floor ( $\times 10^5$ )      | - 0.83         | - 1.30    | - 0.38    | - 2.41    | 0.59      | 0.70      | 0.77      | - 4.17    | - 4.79    | - 2.86    |
| 4th floor ( $\times 10^5$ )      | - 0.90         | - 1.31    | - 1.67    | - 2.47    | - 3.31    | - 1.27    | - 1.14    | 0.29      | - 1.99    | 1.04      |
| 5th floor ( $\times 10^5$ )      | - 0.28         | - 1.14    | - 0.62    | - 1.59    | 1.13      | - 1.13    | 0.49      | - 3.24    | - 0.79    | - 9.79    |
| $J_{avr} (\times 10^5) [mm/s^3]$ | 6.33           | 5.49      | 5.51      | 4.66      | 5.56      | 5.53      | 6.15      | 4.66      | 3.62      | 3.25      |
| Position ( $l_c, h_c$ )          | (600, 20)      | (600, 25) |           |           |           |           |           |           |           |           |
| 2nd floor ( $\times 10^5$ )      | - 0.28         | - 1.06    |           |           |           |           |           |           |           |           |
| 3rd floor ( $\times 10^5$ )      | - 1.25         | - 0.74    |           |           |           |           |           |           |           |           |
| 4th floor ( $\times 10^5$ )      | 0.41           | - 0.34    |           |           |           |           |           |           |           |           |
| 5th floor ( $\times 10^5$ )      | 0.26           | - 1.15    |           |           |           |           |           |           |           |           |
| $J_{avr} (\times 10^5) [mm/s^3]$ | 6.28           | 6.01      |           |           |           |           |           |           |           |           |

**Table 8** Two experimental points set for simulations

|         |  |
|---------|--|
| Point 1 | [(0, - 80) (0, - 40) (0, 0) (0, 40) (0, 80)<br>(300, - 80) (300, - 40) (300, 0) (300, 40) (300, 80)]           |
| Point 2 | [(300, - 80) (300, - 40) (300, 0) (300, 40) (300, 80)<br>(600, - 80) (600, - 40) (600, 0) (600, 40) (600, 80)] |

a combination of  $l_c$  and  $h_c$  for control points 1 and 2, based on the ranges listed in Table 4. In this case, control point 1 is denoted by  $l_{c1}, h_{c1}$  and control point 2 is denoted by  $l_{c2}, h_{c2}$ . The point where the length of  $l_c$  is short from the reference point is referred to as the control point 1, and the point that is long from the reference point is referred to as control point 2. Additionally,  $l_c$  is set as [0 300 600] and  $h_c$  is set as [- 80 - 40 0 40 80]. In Table 8, a combination of these points is presented.

Based on Table 8, 75 simulation models were designed, and the simulations were performed. In this process, 48

experimental points exceeded the maximum design range, i.e., the  $h_p$  constraint in Table 4; thus, modeling was not performed for these points. Furthermore, based on the simulation, it was found that, at 22 of the experimental points, climbing was not feasible and that slipping occurred. Simulated data for the five experimental points are presented in Table 9.

### 4.3 Simulation Results

It is possible to determine the optimal blade spline shape when there is one control point, as in Table 7, and the optimal blade spline shape when there are two control points, as in Table 9. To determine the optimal shape for each case, in this study, the difference between the jerk generated in the initial model and the average jerk generated in the improved shape was considered. When there is one control point,  $l_c, h_c$  is (300, 15); by contrast, when there are

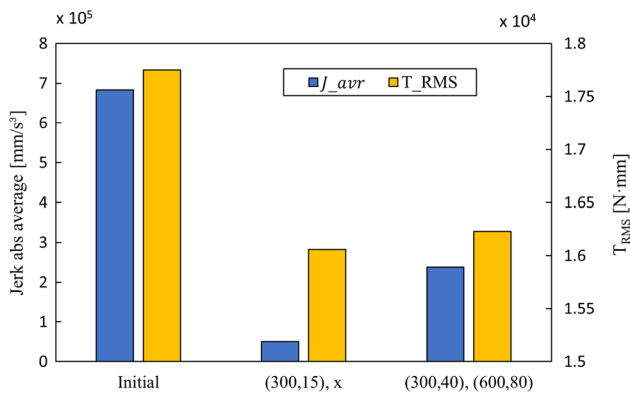
**Table 9** Result of simulation 2 (jerk)

| $(l_{c1}, h_{c1}), (l_{c2}, h_{c2})$ | Initial (0, 0) | (0, - 80), (300, 80) | (0, - 40), (300, 80) | (300, 0), (600, 40) | (300, 0), (600, 80) | (300, 40), (600, 80) |
|--------------------------------------|----------------|----------------------|----------------------|---------------------|---------------------|----------------------|
| 2nd floor ( $\times 10^6$ )          | 0.77           | - 8.40               | - 0.98               | - 0.09              | - 0.68              | - 0.49               |
| 3rd floor ( $\times 10^6$ )          | 0.57           | 3.83                 | - 1.09               | 0.61                | 0.04                | - 0.02               |
| 4th floor ( $\times 10^6$ )          | 0.63           | - 9.29               | - 1.08               | - 0.04              | - 0.92              | - 0.15               |
| 5th floor ( $\times 10^6$ )          | 0.76           | - 8.35               | - 0.90               | 0.35                | - 0.23              | - 0.30               |
| $J_{avr} (\times 10^6) [mm/s^3]$     | -              | - 6.78               | - 0.33               | 0.41                | 0.22                | 0.45                 |



**Table 10** Summarized results of simulation

| $(l_{c1}, h_{c1}), (l_{c2}, h_{c2})$  | Initial model | (300, 15), x | (300, 40) (600, 80) |
|---------------------------------------|---------------|--------------|---------------------|
| Jerk abs average [mm/s <sup>3</sup> ] | 683233        | 50275        | 238719              |
| Friction coefficient                  | 0.46          | 0.51         | 0.68                |
| $T_{RMS}$ [N mm]                      | 17751         | 16061        | 16231               |



**Fig. 6** Summarized results of simulation (Results of  $J_{avr}$  and  $T_{RMS}$ )

two control points,  $(l_{c1}, h_{c2})$  and  $(l_{c2}, h_{c2})$  corresponding to (300,40) and (600,80), respectively, are the most efficient. Accordingly, the average absolute jerk value,  $T_{RMS}$ , and the friction coefficient were compared, and the most optimal model was determined.

The final simulation results are summarized in Table 10 and Fig. 6. Among the two improved models, the model with one control point showed excellent overall efficiency. An improvement of approximately 92% was observed in the average absolute jerk value, and the  $T_{RMS}$  value was also reduced by 1690 N mm. The coefficient of friction required to overcome the stairs slightly increased from 0.46 to 0.51, compared with the friction coefficient of the anti-skid rubber pad applied to the triangular wheel, as shown in Table 3. Thus, it is clear that no issues occurred when overcoming the stairs. Moreover, compared with the initial model, the model with two control points also exhibited good overall results; nevertheless, the results with one control point were better.

**Fig. 7** Prototype robot and blades **a** LEVO prototype robot **b** LEVO with B-spline(one control point) blade and its blade **c** LEVO with B-spline(two control point) blade and its blade



## 5 Experimental Verification

As discussed in the previous section, we conducted a simulation to reduce the jerk that occurs when the robot collides with stairs. Based on this, it was possible to determine the optimal B-spline shape; however, it is still necessary to prove whether this approach is effective under actual environments. To this end, a prototype of LEVO and the two blades derived from previous simulations were manufactured and tested. In the previous simulations, the efficiency of the blade was verified using three parameters: jerk,  $T_{RMS}$ , and the friction coefficient. However, in an actual environment, it is difficult to measure the value of  $T_{RMS}$  and the coefficient of friction required to overcome stairs. Therefore, using the BWT901C 9-axis accelerometer, we only measured the jerk and compared its values to verify the reliability of the simulation. The calculation and derivation of the jerk values are as follows. The steps measured by the IMU sensor and the acceleration of the robot before the blade collides with the change in acceleration immediately after the collision were divided by the sensor’s sampling time.

### 5.1 Prototype of the ROBOT

The manufactured prototype robots and the shape of the robots’ blade are presented in Fig. 7. Based on the basic model of (a), (b) shows a (300,15) blade and assembly shape of LEVO with B-spline (one control point), and (c) shows a (300,40)(600,80) blade and assembly shape of LEVO with B-spline (two control points). The overall size of the robot was 700 mm  $\times$  870 mm  $\times$  398 mm, and its total mass was 20 kg.

The CSTW, designed to fit the dimensions of the stairs, was manufactured using ABS plastic. Here, the CSTW was primarily composed of spokes and stoppers. The spoke structure enables the robot to climb stairs, whereas rubber pads are attached to increase the friction with the stairs. Additionally, a stopper mechanism [16] was employed to enable the CSTW to climb stairs of different sizes.

The blade was coupled with the lower part of the robot body, as shown in Fig. 7b and c. To obtain the exact shape

of the blade, two optimized shapes derived from the simulation results were converted into drawings. Based on these drawings, the blade was prepared from acrylic resin using a laser cutter.

In the experimental verification, an IMU sensor was attached to the center of gravity of the robot to measure the acceleration that occurs when the stairs and blades collide. This measured acceleration was used to induce jerk, a change in acceleration. The IMU sensor used in the experiment used the WT901C model, a 9DOF measurement sensor module. The sampling rates for the above sensors are 115200bps and 100 Hz. The experimental results were derived by processing the output data.



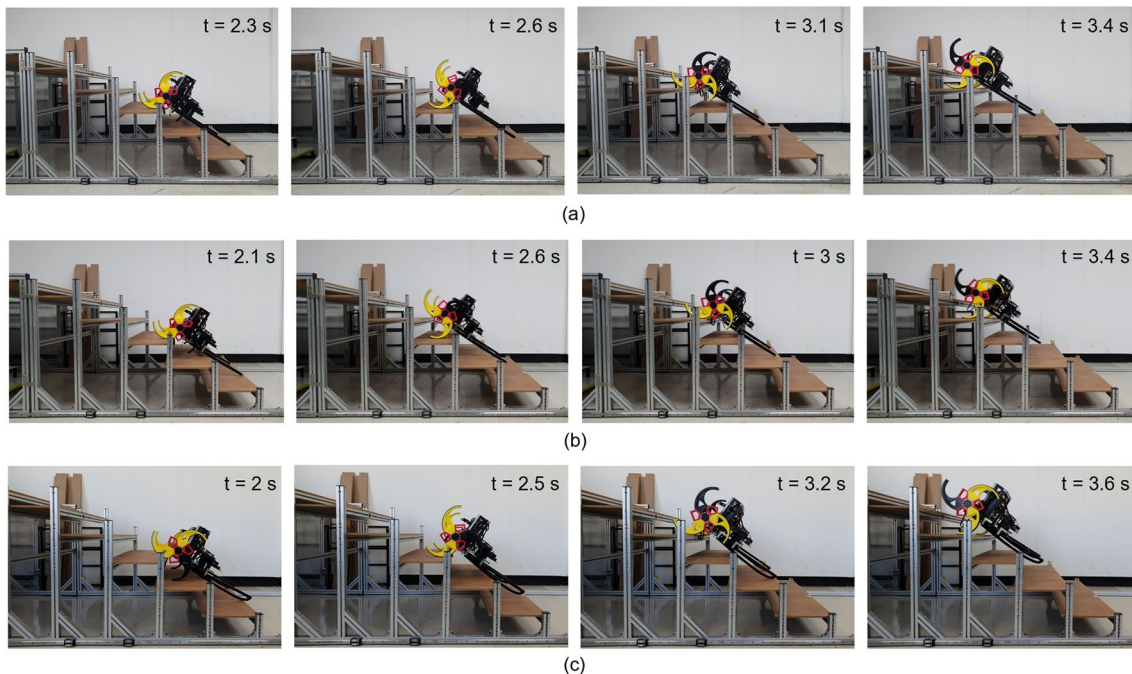
**Fig. 8** Test bench (300 mm×160 mm)

## 5.2 Experiment Results

To proceed with the experiment, test bench stairs that were suitable owing to their size were employed. The shape of the manufactured test bench is depicted in Fig. 8; it was manufactured using MDF plywood and an aluminum profile to fit the 300 mm×160 mm dimensions of the staircase, which was the target in this study. The prototype robot described above was operated on this test bench, and the jerk values were determined based on the values read from the accelerometer. The results thus obtained when then compared.

As shown in Fig. 9, the experiment was conducted using a test bench. The jerk values that occurred when the floor of the robot collided with the 2nd, 3rd, and 4th steps of the stairs were measured, and the results were compared with the simulation values. Figure 9 shows the process of collision with the 2nd and 3rd steps.

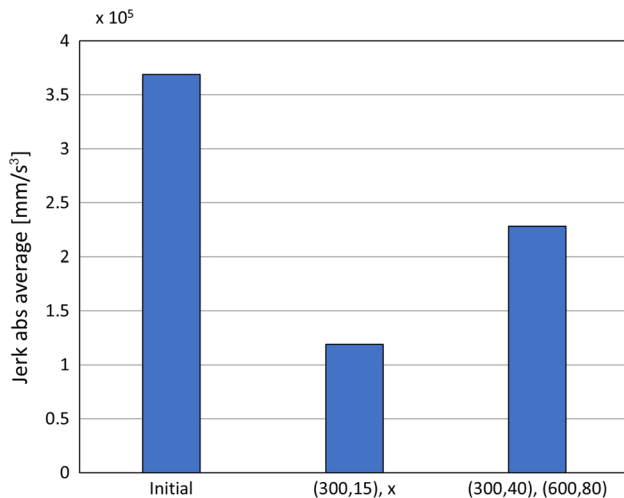
Thus, the results listed in Table 11 and Fig. 10 were obtained. The two optimal blade shapes were verified in an actual environment. As a result of this verification, similar to the simulations, the best results were obtained for the shape with one control point. The case with one control point afforded a decrease of 66.7% in the jerk value, as compared with the initial model, whereas the case with two control points showed a decrease of 38.2% in the jerk value. Variables such as the frictional force tend to vary owing to dust or surface treatments, which may be present in actual environments; however, these conditions could not be replicated



**Fig. 9** Experimental results: **a** initial model, **b** one control point blade, **c** two control points blade

**Table 11** Summarized experimental results

| Kind of blade<br>( $l_{c1}, h_{c1}$ ), ( $l_{c2}, h_{c2}$ ) | Initial | (300, 15), x | (300, 40) (600, 80) |
|---|---------|--------------|---------------------|
| Jerk:2nd floor ( $\times 10^5$ )                            | - 2.13  | - 1.27       | 2.31                |
| Jerk:3rd floor ( $\times 10^5$ )                            | - 3.72  | - 1.66       | 1.45                |
| Jerk:4th floor ( $\times 10^5$ )                            | 4.43    | 0.65         | - 3.09              |
| Jerk abs average<br>( $\times 10^5$ ) [ $\text{mm/s}^3$ ]   | 3.69    | 1.19         | 2.28                |

**Fig. 10** Summarized experimental results (Result of Jerk abs average)

in this verification. Nevertheless, the decrease in the jerk value remains significant.

## 6 Conclusion

This study aimed to reduce the jerk that occurs when a robot using CSTW climbs stairs. Previous results confirmed that the amount of jerk generated by attaching a curved surface such as a B-spline curve to the robot floor can be reduced by about 92% in simulation and 66.7% in real-world verification. This in turn can extend the service life of such robots as mentioned earlier in the white paper. Also, when applied to last mile delivery platforms, this approach can potentially provide higher quality delivery services due to the benefits of vibration reduction.

In this study, optimization was performed considering only one dimension of the stairs. In the future, we plan to robustly optimize the B-spline curve of the blade so that it can be applied simultaneously to stairs with different dimensions that are often used. And this optimization proceeds with a robust optimization of the previous CSTW. In addition, in the actual environmental test verification process of this

study, not only jerk but also driving torque and minimum required friction coefficient are measured as evaluation items through the configuration of an additional test bench to further increase the reliability of verification.

**Acknowledgements** This work is supported by a Korea Agency for Infrastructure Technology Advancement(KAIA) grant funded by the Ministry of Land, Infrastructure, and Transport (Grant 21CTAP-C164242-01).

## Declarations

**Competing interests** The authors declare that they have no conflict of interest.

## References

1. Covid-19 accelerates e-commerce growth in south korea, says globaldata. GlobalData (2020).
2. Joerss, M., Neuhaus, F., & Schröder, J. (2016). How customer demands are reshaping last-mile delivery. *The McKinsey Quarterly*, 17, 1–5.
3. Global last mile delivery market: Industry analysis and forecast (2021–2027). MAXIMIZE(MARKET RESEARCH PVT.LTD.) (2020).
4. Chen, C., Demir, E., Huang, Y., & Qiu, R. (2021). The adoption of self-driving delivery robots in last mile logistics. *Transportation Research Part E: Logistics and Transportation Review*, 146, 102214.
5. Panwar, V. S., Pandey, A., & Hasan, M. E. (2021). Motor velocity based multi-objective genetic algorithm controlled navigation method for two-wheeled pioneer p3-dx robot in v-rep scenario. *International Journal of Information Technology*, 13(5), 2101–2108.
6. Holt, K. (2019). Amazon starts testing its ‘scout’ delivery robot:it’s delivering packages to customers in a washington neighborhood starting today. engadget.
7. Jung, J. (2021). Hyundai, woowa expand automated vehicle with new contact-free delivery robots. koreatechtoday.
8. Ilyas, M., Yuyao, S., Mohan, R. E., Devarassu, M., & Kalimuthu, M. (2018). Design of stetro: A modular, reconfigurable, and autonomous staircase cleaning robot. *Journal of Sensors*. <https://doi.org/10.1155/2018/8190802>
9. Megalingam, R.K., Prem, A., Nair, A.H., Pillai, A.J. & Nair, B.S. (2016). Stair case cleaning robot: Design considerations and a case study. In *2016 International Conference on Communication and Signal Processing (ICCSP)*, pp. 0760–0764. IEEE.
10. Calderone, L. (2019). Boston dynamics’ spotmini robot and more. ROBOTICS TOMORROW.
11. Raibert, M., Blankespoor, K., Nelson, G., & Playter, R. (2008). Bigdog, the rough-terrain quadruped robot. *IFAC Proceedings Volumes*, 41(2), 10822–10825.
12. Zhang, Q., Ge, S.S. & Tao, P.Y. (2011). Autonomous stair climbing for mobile tracked robot. In *2011 IEEE International Symposium on Safety, Security, and Rescue Robotics*, pp. 92–98. IEEE.
13. Son, D., Shin, J., Kim, Y., & Seo, T. (2022). Levo: Mobile robotic platform using wheel-mode switching primitives. *International Journal of Precision Engineering and Manufacturing*, 23(11), 1–10.
14. Shin, J., Son, D., Kim, Y., & Seo, T. (2022). Design exploration and comparative analysis of tail shape of tri-wheel-based stair-climbing robotic platform. *Scientific Reports*, 12(1), 19488.

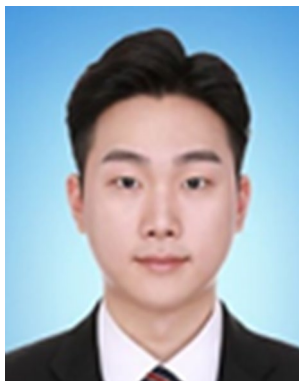
15. Shin, J., Kim, Y., Kim, D.-Y., Yoon, G. H., & Seo, T. (2023). Parametric design optimization of a tail mechanism based on tri-wheels for curved spoke-based stair-climbing robots. *International Journal of Precision Engineering and Manufacturing*. <https://doi.org/10.1007/s12541-023-00817-4>
16. Kim, Y., Kim, J., Kim, H. S., & Seo, T. (2019). Curved-spoke tri-wheel mechanism for fast stair-climbing. *IEEE Access*, 7, 173766–173773.
17. Gasparetto, A., & Zanotto, V. (2008). A technique for time-jerk optimal planning of robot trajectories. *Robotics and Computer-Integrated Manufacturing*, 24(3), 415–426.
18. Qiu, H., Lin, C.-J., Li, Z.-Y., Ozaki, H., Wang, J., & Yue, Y. (2005). A universal optimal approach to cam curve design and its applications. *Mechanism and Machine Theory*, 40(6), 669–692.
19. Dippel, S., Batrouni, G., & Wolf, D. (1996). Collision-induced friction in the motion of a single particle on a bumpy inclined line. *Physical Review E*, 54(6), 6845.
20. Gordon, W. J., & Riesenfeld, R. F. (1974). *B-spline curves and surfaces*, 95–126.
21. Hassan, M. (2013). Optimization of stay cables in cable-stayed bridges using finite element, genetic algorithm, and b-spline combined technique. *Engineering Structures*, 49, 643–654.
22. Hedayat, A.S., Sloane, N.J.A. & Stufken, J. (1999). Orthogonal arrays: theory and applications.

**Publisher's Note** Springer Nature remains neutral with regard to jurisdictional claims in published maps and institutional affiliations.

Springer Nature or its licensor (e.g. a society or other partner) holds exclusive rights to this article under a publishing agreement with the author(s) or other rightsholder(s); author self-archiving of the accepted manuscript version of this article is solely governed by the terms of such publishing agreement and applicable law.



**Younghwan Kim** received his B.S. degree in Mechanical Engineering from Hanyang University in 2022. He is currently working toward his M.S. degree in Mechanical Engineering at Hanyang University. His research interests lie in the design of robot mechanisms.



**Donghan Son** received his B.S degree in mechanical engineering from Kookmin University in 2020 and M.S degrees in Mechanical Engineering at Hanyang University in 2022. His research interests lie in the areas of robot mechanism design.



**Jeongpil Shin** received his B.S degree in Mechanical Engineering from Hanyang University in 2020. He is currently working toward his M.S. degree in Mechanical Engineering at Hanyang University. His research interests lie in the design of robot mechanisms.



**Taewon Seo** received B.S. and Ph.D. degrees from the School of Mechanical and Aerospace Engineering, Seoul Nat'l Univ., Korea in 2003 and 2008, respectively. He is a professor at the School of Mechanical Engineering, Hanyang University, South Korea. Before Hanyang University, he was a postdoctoral researcher at Nanorobotics Laboratory, Carnegie Mellon University, a visiting professor at Biomimetic Millisystems Lab., UC Berkeley, a visiting scholar at the University of Michigan, and an

associate professor at the School of Mechanical Engineering, Yeungnam University, South Korea. His research interests include robot design, analysis, control, optimization, and planning. Dr. Seo received the Best Paper Award of IEEE/ASME Transaction on Mechatronics in 2014. He is a Technical/Associate Editor of IEEE/ASME Transaction on Mechatronics and Intelligent Service Robots and was an Associate Editor of IEEE Robotics and Automation Letters.